IVYSPRING INTERNATIONAL PUBLISHER

International Journal of Biological Sciences

2027; 23(2): 705-719. doi: 10.7150/ijbs.139343

Research Paper

Spatiotemporal Lineage Tracing Reveals Molecular and Spatial Heterogeneity in Cochlear Sensory Epithelium

Mingxuan Wu[1,2,3,4#], Jiacheng Fan[6#], Yuyan Gu[1], Yuqiu Zhou[6], Tianshi Sun[7], Yaoqian Liu[1,2,3,4], Gaogan Jia[1,2,3,4], Jinjie Yang[7], Yiyun Lou[1,2,3,4], Yunjie Li[1,2,3,4], Huawei Li[1,2,3,4,5], Wenquan Li[8]✉, Yan Chen[1]✉, Ying Zhu[6]✉, Wenyan Li[1,2,3,4,5]✉

1. ENT institute and Otorhinolaryngology Department of Eye & ENT Hospital, State Key Laboratory of Medical Neurobiology and MOE Frontiers Center for Brain Science, Fudan University, Shanghai, 200031, China.
2. Institutes of Biomedical Sciences, Fudan University, Shanghai 200032, China.
3. NHC Key Laboratory of Hearing Medicine, Fudan University, Shanghai 200032, China.
4. The Institutes of Brain Science and the Collaborative Innovation Center for Brain Science, Fudan University, Shanghai 200032, China.
5. Shanghai Engineering Research Centre of Cochlear Implant, Shanghai 200031, China.
6. State Key Laboratory of Brain Function and Disorders, MOE Frontiers Center for Brain Science, Fudan University, Shanghai. China.
7. School of Life Sciences, Zhejiang Chinese Medical University, Hangzhou, 310053, China.
8. Department of Otolaryngology, The Second Affiliated Hospital of Soochow University, Suzhou, 215004, China.

#These authors contributed equally: Mingxuan Wu and Jiacheng Fan

✉ Corresponding authors: wenyan_li@fudan.edu.cn (W.Y. L.); ying_zhu@fudan.edu.cn (Y. Z.); chenyan0528@fudan.edu.cn (Y. C.); liwq2025@126.com (W.Q. L.).

© 2027 The Author(s). This is an open access article distributed under the Creative Commons Attribution 4.0 International Licence, subject to the Publisher's Terms of Use at https://ivyspring.com/terms.

Received: 2026.06.14; Accepted: 2026.10.24; Published: 2027.01.01

Abstract

Coordinated cell proliferation, differentiation, and migration are fundamental to cochlear morphogenesis. However, the cellular origins of the organ of Corti and the mechanisms guiding medial (neural) -lateral (abneural) axis patterning remain incompletely understood. Cochlear prosensory cells (CPCs) are the prosensory epithelial population that gives rise to hair cells (HCs) and supporting cells (SCs). Using single-cell RNA sequencing and morphological analyses, we uncovered intrinsic heterogeneity within mouse CPCs along the medial-lateral axis: *Jag1*$^+$ CPCs localize to the medial region, *Cdkn1b*$^+$ CPCs reside laterally, and the two populations overlap in an intermediate zone where cells co-express *Jag1* and *Cdkn1b*. Time-lapse imaging revealed *Jag1*$^+$ and *Cdkn1b*$^+$ CPCs migrate toward each other along the medial-lateral axis, converging and intercalating to establish the checkerboard-like organization of the organ of Corti. Furthermore, sequential lineage tracing using a dual recombinase system demonstrated that cells sequentially expressing *Jag1* and *Cdkn1b* differentiate into both HCs and their associated SCs, confirming their identity as prosensory precursors. Notably, comparative analysis of human cochlea revealed conserved expression and patterning mechanisms, suggesting evolutionary preservation of this developmental program. Collectively, our findings establish that the assembly of the organ of Corti is driven by the coordinated differentiation and intercalating migration of spatially and molecularly distinct prosensory populations along the cochlear medial-lateral axis —a principle that appears to be evolutionarily conserved across mammals.

Introduction

The mammalian cochlea is a highly specialized sensory organ responsible for auditory perception. It arises from the otic placode, a thickened region of non-neuroectoderm adjacent to the hindbrain, which undergoes invagination and detachment from the ectoderm to form the otocyst [1-3]. Early patterning of the otocyst is established along three primary axes (dorsoventral, anteroposterior, and mediolateral) via morphogen gradients, including Wnt [4], Sonic hedgehog (SHH) [5], retinoic acid (RA) [6], and fibroblast growth factor (FGF) signaling [7], which drive the specification of the ventromedial otocyst into the cochlear primordium [8,9]. In mice, between E11.5 and E18.5, the cochlear duct undergoes dramatic morphogenetic remodeling, including cell proliferation, epithelial thickening, and outgrowth,

ultimately forming the characteristic spiral structure of the cochlea with its distinctive checkerboard-like cellular architecture [10]. The cochlear roof gives rise to Reissner's membrane and stria vascularis [11], while the cochlear floor differentiates into the sensory epithelium, which contains the organ of Corti [12]—the functional unit responsible for mechanoelectrical transduction in hearing. In neonatal mice, the cochlear sensory epithelium comprises the organ of Corti, the medial (neural) Kolliker's organ, and the lateral (abneural) lesser epithelial ridge. As cochlear maturation proceeds and functional auditory circuits are established, Kolliker's organ and lesser epithelial ridge gradually regress and differentiate into inner and outer sulcus cells, respectively [13-15].

The organ of Corti exhibits a highly organized structure with distinct mediolateral compartments (Figure 1A). The medial (neural) region contains inner hair cells (IHCs) and their associated supporting cells, including inner border cells (IBCs), inner phalangeal cells (IPhCs), and inner pillar cells (IPCs). The lateral (abneural) compartment consists of outer hair cells (OHCs) together with outer pillar cells (OPCs), Deiters cells (DCs), and Hensen cells (HeCs). These two compartments are separated by the tunnel of Corti (TC), the development of which is regulated by Connexin 26[16]; loss of Connexin 26 leads to profound hearing loss and TC structural malformation, which can be rescued by viral-mediated Connexin 26 expression[17]. Accumulating evidence indicates that cochlear prosensory cells (CPCs) are not a homogeneous population, but instead exhibit regional and molecular heterogeneity [18]. Notably, OHCs and surrounding SCs derive from a distinct *Tgfβr1*$^{+}$ precursor pool localized to the lateral (abneural) cochlear domain [18]. Several transcriptional regulators also have been implicated in hair cell subtype specification: *Insm1* [19] and *Ikzf2* [20] promote OHC differentiation, while *Tbx2* [21,22] and *Casz1* [23] are associated with IHC fate. Our previous work revealed regional differences in the regenerative capacity of SCs across the cochlear epithelium, with lateral (abneural) SCs preferentially converting to OHCs and medial (neural) SCs to IHCs following overexpression of *Gfi1/Pou4f3/Atoh1* [24]. These findings underscore the existence of multiple, lineage-restricted CPC subpopulations, although the full spectrum of cellular heterogeneity in the cochlear prosensory epithelium remains poorly characterized.

Cochlear duct elongation and morphogenesis involve complex three-dimensional epithelial reorganization, including coordinated apical-basal extension, convergent extension, and torsional outgrowth [4,25,26]. These processes are driven by coordinated cell proliferation and extensive cell migration mediated by myosin II contractility [10,27]. Cochlear extension is regulated by SHH [5,28], FGF [29], and canonical Wnt-planar cell polarity (PCP) signaling [30]. Large-scale cellular shear motion facilitates cochlear duct extension along the apex-base axis and mediolateral narrowing via convergent extension [10,31]. While these pathways contribute to overall duct elongation and domain patterning, the precise migratory behaviors of CPCs and the mechanisms directing domain-specific differentiation within the organ of Corti remain incompletely understood.

In this study, we identified that medial (neural) and lateral (abneural) CPCs can be distinguished as early as E12.5 and characterized their dynamic, stage-dependent gene expression profiles during cochlear development. To dissect the molecular heterogeneity of the cochlear sensory epithelium, we established a novel dual-recombinase-mediated lineage tracing system that utilizes two distinct promoters to sequentially label cells with fluorescent reporters according to their temporal gene expression patterns. This approach not only enables high-resolution mapping of CPC contributions to cochlear epithelial development but also provides a versatile platform for investigating cellular behaviors during both development and regeneration processes. A key advantage is its capacity to unambiguously identify newly generated HCs or neurons through stage-specific multi-marker labeling—a feature unattainable with conventional single-gene-based strategies. Using transgenic animal models combined with this dual-recombinase system, we have systematically validated the spatial and molecular heterogeneity within the developing cochlear sensory epithelium. Furthermore, our results reveal previously uncharacterized mechanisms underlying cellular convergence and migration along the medial (neural) -lateral (abneural) axis during cochlear duct differentiation, offering critical insights into the complex morphogenetic processes shaping the auditory sensory organ.

Results

Single-cell transcriptional profiling revealed heterogeneity of prosensory cells in developing cochlear epithelium

The mammalian cochlea exhibits a highly organized cellular architecture, with sensory HCs and SCs arranged in curvilinear rows along the tonotopic axis while displaying divergent polarization along the mediolateral axis (Figure 1A). During mouse embryogenesis, the cochlear duct primordium arises from ventromedial thickening and sprouting of the otocyst epithelium, ultimately elongating and coiling into a mature 2.5-turn spiral structure (Figure 1B).

Early CPCs undergo rapid expansion before progressively exiting the cell cycle in an apex-to-base gradient [32], a pattern confirmed by our Ki67 immunostaining results (Figure 1C, Figure S1A, B). Lineage tracing results demonstrated that the *Sox2*$^{+}$ CPCs in the prosensory epithelium (E12.5–E13.5) give rise to 90–100% of cochlear HCs and their associated SCs [33]. Despite uniform *Sox2* expression across the prosensory domain (Figure S1C), we observed striking regional disparity between medial (neural) and lateral (abneural) CPCs using Ki67 immunostaining. While the propagation of the "end-proliferation" signal spreads from apex to base [32], a concurrent mediolateral gradient is evident, with medial (neural) CPCs retaining Ki67 expression from E12.5 to E14.5 (Figure 1C), suggesting intrinsic differences in CPC biology.

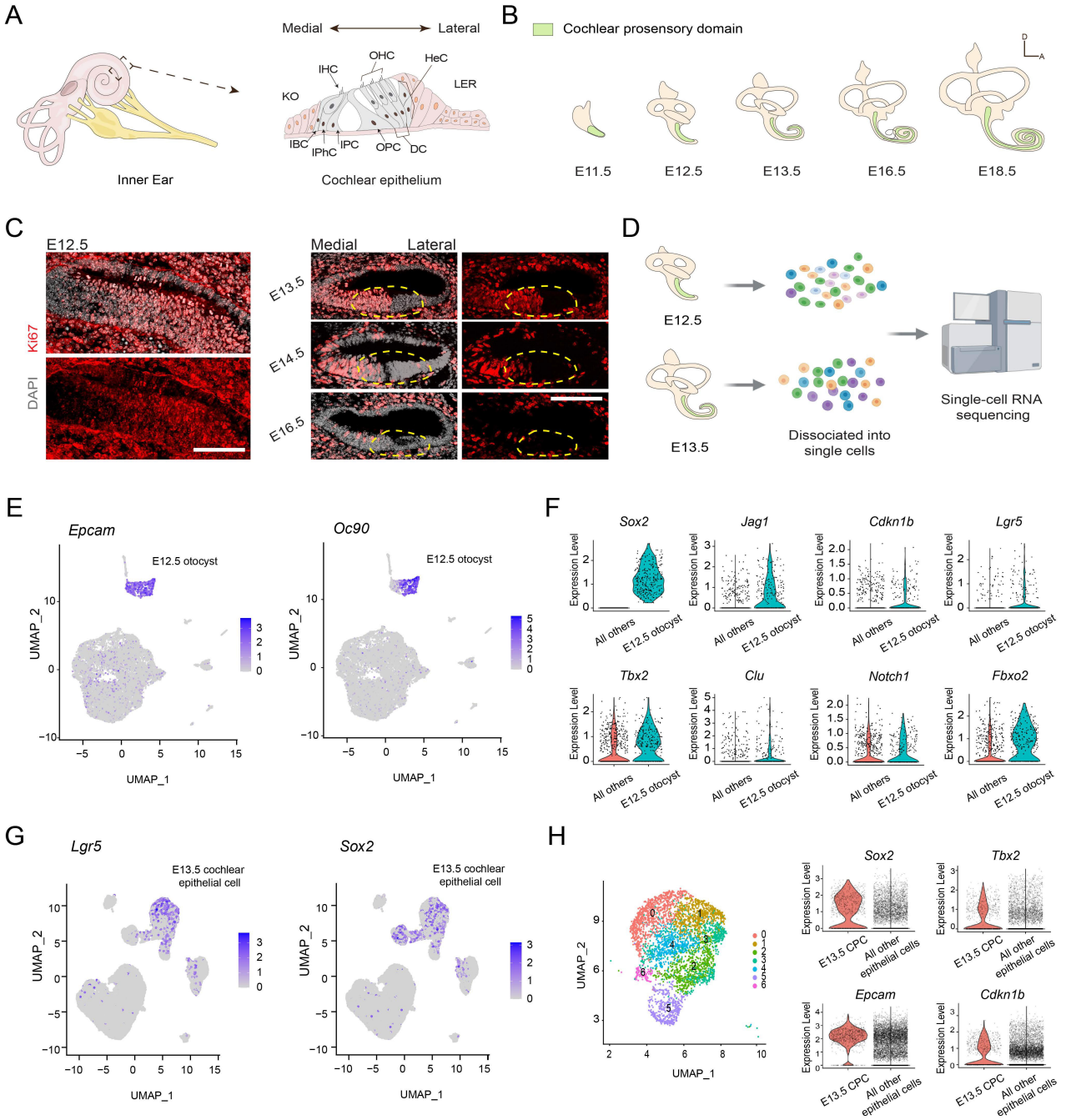


Figure 1. Cochlear Development Overview and Single-Cell Transcriptomic Analysis of Cochlear Development at E12.5 and E13.5. (A) Schematic of the mouse inner ear anatomy and cellular composition of the organ of Corti. (B) Morphogenetic extension of the prosensory epithelium during embryonic cochlear development. (C) Ki67 immunofluorescence showed regional disparity between medial (neural) and lateral (abneural) cochlear prosensory cells (CPCs). CPC localizations are indicated by yellow dashed circles. Scale bar: 50 μm. (D) Experimental workflow for single-cell RNA sequencing of the developing cochlear epithelium. (E) Identification of E12.5 cochlear epithelium using *Epcam* and *Oc90* expression. (F) Violin plots showing prosensory gene expression in E12.5 otocyst compared to other cell populations. (G) Characterization of E13.5 cochlear epithelium by *Lgr5* and *Sox2* expression. (H) Unsupervised clustering of E13.5 cochlear epithelial cells. Violin plots display prosensory gene expression in *Sox2*$^{+}$ CPCs relative to other epithelial cells. Abbreviations: IHC, inner hair cell; OHC, outer hair cell; IBC, inner border cell; IPhC, inner phalangeal cell; IPC, inner pillar cell; OPC, outer pillar cell; DC, Deiters' cell; HeC, Hensen's cell; KO, Kolliker's organ; LER, lesser epithelial ridge.

To comprehensively define CPC identities and fate commitment mechanisms, we isolated E12.5 and E13.5 cochleae for single-cell RNA-seq (Figure 1D). At E12.5, cochlear epithelial cells were identified by epithelial markers (*Epcam*, *Oc90*) and exhibited high levels of prosensory-associated genes, including *Sox2*, *Jag1*, *Cdkn1b*, and *Lgr5* (Figure 1E, F). Gene ontology (GO) analysis further confirmed their sensory precursor identity, with markers enriched in "Sensory perception of sound", "Mechanosensory transduction", and "Sensory organ morphogenesis" (Figure S2A). By E13.5, cochlear epithelial cells were marked by *Sox2* and *Lgr5* (Figure 1G), and unsupervised clustering revealed seven transcriptionally distinct subpopulations within cochlear epithelial cells (Figure 1H, Figure S1D).

To construct a comprehensive transcriptional atlas of cochlear development, we integrated our E12.5 and E13.5 *Sox2*$^+$ CPC dataset with publicly available datasets from E14 and E16 cochleae [18] (Figure 2A). Quality control metrics, including nFeature RNA, nCount RNA, and mitochondrial RNA percentage, were summarized for each library across embryonic stages E12.5, E13.5, E14, and E16 before and after filtering (Figure S2B). Unsupervised clustering analysis revealed 11 distinct cell populations with unique molecular signatures, while Monocle2 pseudotime analyses delineated the divergence of E12.5–E13.5 CPCs into E14 medial (neural) and lateral (abneural) prosensory cells (M.PsCs and L.PsCs), (Figure 2B, C) that ultimately give rise to E16 inner hair cells (IHCs) and outer hair cells (OHCs) (Figure 2D), respectively. However, pseudotime analysis alone could not fully resolve this lineage trajectory (Figure 2D).

Pseudotemporal analysis from E12.5 through E16 demonstrated a progressive downregulation of prosensory genes coupled with sequential activation of SC and HC markers as cells mature (Figure 2E). To determine region-specific prosensory cells, we further examined the differentially expressed genes, including *Tbx2, Jag1*, *Tgfbr1*, and *Cdkn1b* (Figure 2F, G). We noticed within E12.5 and E13.5 prosensory cells, *Tbx2* (an IHC fate determinant) and *Jag1* exhibited congruent expression patterns, as did *Tgfbr1* (a lateral precursor marker) and *Cdkn1b* (Figure 2F, G). These co-expression profiles suggest *Jag1* and *Cdkn1b* may serve as reliable markers for medial (neural) and lateral (abneural) CPC subpopulations, respectively, thus refining our understanding of regional fate specification.

The cochlear prosensory epithelium exhibits distinct medial (neural) -lateral (abneural) patterning

JAG1, a Notch ligand critical for inner ear sensory specification[34,35], initiates expression at E10.5 and serves as a pivotal CPC marker [34]. However, *Jag1* exhibits non-uniform distribution across the prosensory epithelium; it preferentially labels a medial (neural) CPC subpopulation that partially overlaps with the *Cdkn1b*-expressing domain at its lateral (abneural) boundary[36]. Notably, *Cdkn1b,* which encodes the cyclin-dependent kinase inhibitor p27Kip1, demarcates a zone of non-proliferating cells that ultimately gives rise to the organ of Corti[32]. While *Jag1* and *Cdkn1b* show partial co-expression in E13.5 CPCs (Figure 3A; note the yellow *Jag1*$^+$/*Cdkn1b*$^+$ cells), the developmental fate of these overlapping cell populations remains unresolved.

To investigate this regional specificity, we generated *Jag1*-iCreERT2 (V5-tagged) and *Cdkn1b*-Flpo (HA-tagged) mouse lines using the CRISPR/Cas9 system (Figure 3B), and crossed them to characterize the overlapping expression of *Jag1* and *Cdkn1b* (Figure 3C). Immunostaining confirmed faithful colocalization of V5 with JAG1 and HA with p27Kip1 in the cochlear sensory epithelium (Figure 3E, F), thus validating recombinase fidelity. *Jag1*$^+$ CPCs were located medially, while *Cdkn1b*$^+$ CPCs were located laterally in the E13.5 cochlear prosensory epithelium. Strikingly, CPCs co-expressing *Jag1* and *Cdkn1b* formed a narrow stripe within the prosensory domain (Figure 3D; the zone between the dashed lines), demonstrating that medial (neural) *Jag1*$^+$ CPCs partially overlap with lateral (abneural) *Cdkn1b*$^+$ CPCs along the mediolateral axis.

Jag1$^+$ CPCs give rise to the medial (neural) cochlear epithelium and establish the lateral (abneural) boundary of the organ of Corti

Through lineage tracing in *Jag1*-iCreERT2; *Rosa26*-tdTomato mice (Figure 4A), we systematically investigated the developmental fate of *Jag1*$^+$ CPCs (Figure 4B). A single dose of tamoxifen was administered at E11.5, E12.5, E13.5, or E14.5 to label *Jag1*$^+$ CPCs, and cochleae were dissected at E15.5 or E18.5. When tracing was initiated at E12.5 and cochleae were harvested at E15.5, *Jag1*-tdTomato$^+$ traced cells were predominantly localized to the medial cochlear epithelium. The *Jag1*-tdTomato$^+$ region partially overlaps with the *Sox2*$^+$ prosensory domain, with its lateral boundary confined within the *Sox2*$^+$ domain (indicated by dashed lines; Figure 4C, D). The p27Kip1$^+$ zone (shown by green fluorescence in Figure 4C) was located in the lateral part of the cochlear epithelium, with partial overlap with the

Jag1-tdTomato$^+$ zone (Figure 4C). The developing organ of Corti contained three distinct cell populations: *Jag1*$^+$ cells, *Cdkn1b*$^+$ cells, and a subset co-expressing both markers (Figure 4C, D). Live imaging of *Jag1*-tdTomato$^+$ cells (tracing initiated at E12.5, analyzed at E14.5) demonstrated their dynamic lateral migration during development (Figure 4E, Video 1).

At E18.5, the cochlear sensory epithelium consists of, from medial to lateral, Kölliker's organ, the organ of Corti, and the lesser epithelial ridge. Within the organ of Corti, outer hair cells (OHCs), inner hair cells (IHCs), and their surrounding supporting cells have already differentiated. Analysis at E18.5 following tamoxifen administration at E11.5–E14.5 showed that *Jag1*-tdTomato labeled cells were located in the medial part of the cochlear epithelium, including Kölliker's organ and the organ of Corti (Figure 4F, G). Early tracing (E11.5–E12.5) labeled approximately 90% of IHCs and over 80% of IBCs and IPhCs (Figure S3A, B), whereas later tracing (E13.5–E14.5) showed markedly reduced labeling efficiency (Figure 4H–J), consistent with the early role of *Jag1* in epithelial patterning. Within the organ of Corti, we observed a medial-to-lateral gradient in labeling efficiency, with the highest rates in IHCs and medial supporting cells, and progressively lower rates in OHCs and their associated supporting cells. This gradient, combined with live imaging data, suggests a lateral migration

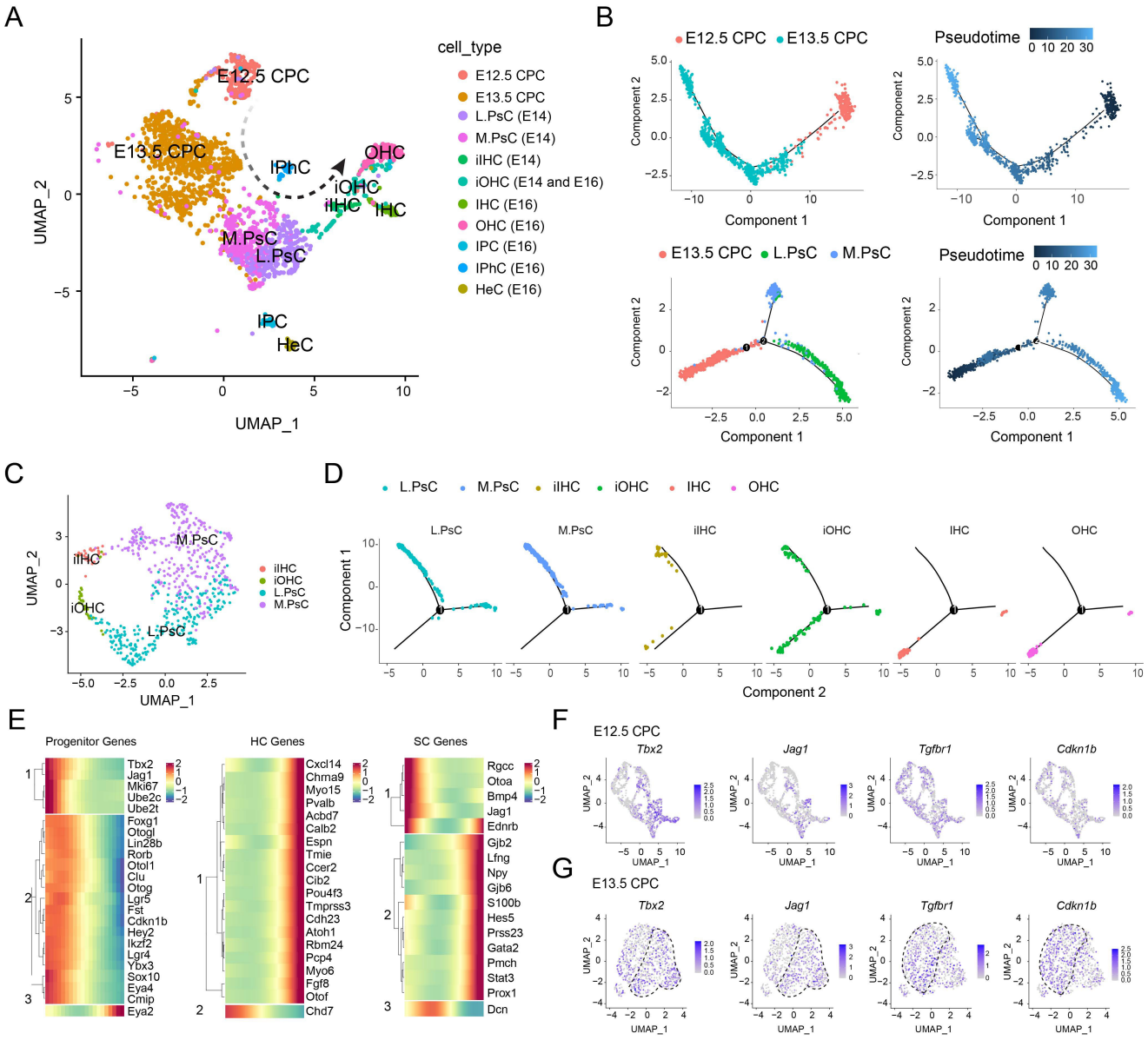


Figure 2. Integrated Single-Cell Transcriptomics Reveal Divergent Lineage Trajectories of Medial (neural) and Lateral (abneural) Cochlear Prosensory Cells (CPCs). (A) Unsupervised clustering of cells from the developing auditory epithelium across stages E12.5 to E16. (B) Developmental trajectory inference from E12.5 and E13.5 CPCs to medial and lateral prosensory cells (M.PsCs and L.PsCs). (C, D) Unbiased clustering (C) and pseudotemporal trajectory analysis (D) of M.PsCs and L.PsCs differentiating into IHCs and OHCs. (E) Dynamic gene expression changes along pseudotime, analyzed using Monocle. (F, G) UMAP visualization of regionally enriched marker genes in E12.5 (F) and E13.5 (G) CPC clusters.

tendency of *Jag1*$^+$ cells. Extensive *Jag1*-tdTomato labeling was present in the medial non-sensory cells of Kölliker's organ, whereas only rare tdTomato$^+$ cells were detected in the lateral lesser epithelial ridge following tamoxifen administration (Figure 4F, G, and S3). Together, these findings establish *Jag1*$^+$ CPCs as a medial (neural) precursor population during early development that gives rise to Kölliker's organ and the organ of Corti, and demarcates the lateral (abneural) boundary of the organ of Corti during cochlear morphogenesis.

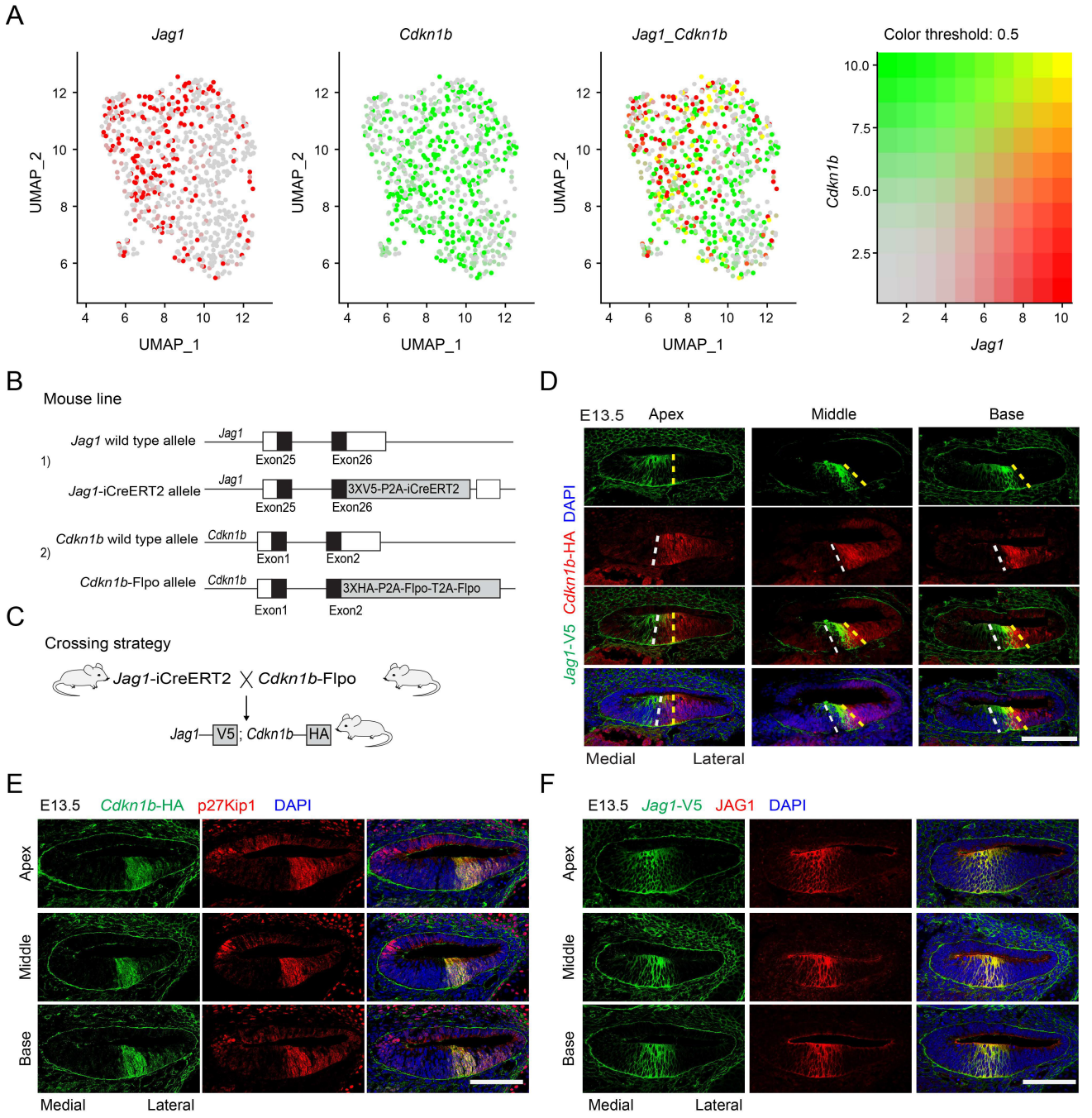


Figure 3. Spatially Distinct Expression of *Jag1* and *Cdkn1b* Along the Medial (neural) -Lateral (abneural) Axis of the Cochlear Prosensory Epithelium. (A) Overlapping yet spatially biased expression patterns of *Jag1* and *Cdkn1b* during cochlear prosensory cell (CPC) development. (B, C) Genetic targeting strategy and mouse crossing scheme for visualization of *Jag1* and *Cdkn1b* expression. (D) Regional specificity of *Jag1*$^+$CPCs in the medial zone and *Cdkn1b*$^+$CPCs in the lateral zone of the prosensory epithelium. The region between yellow (lateral boundary) and white dashed lines (medial boundary) indicates overlapping expression. Scale bar: 50 μm. (E, F) In vivo validation of *Jag1* and *Cdkn1b* promoter-driven recombinase expression via V5 and HA immunostaining at E13.5. Scale bars: 50 μm.

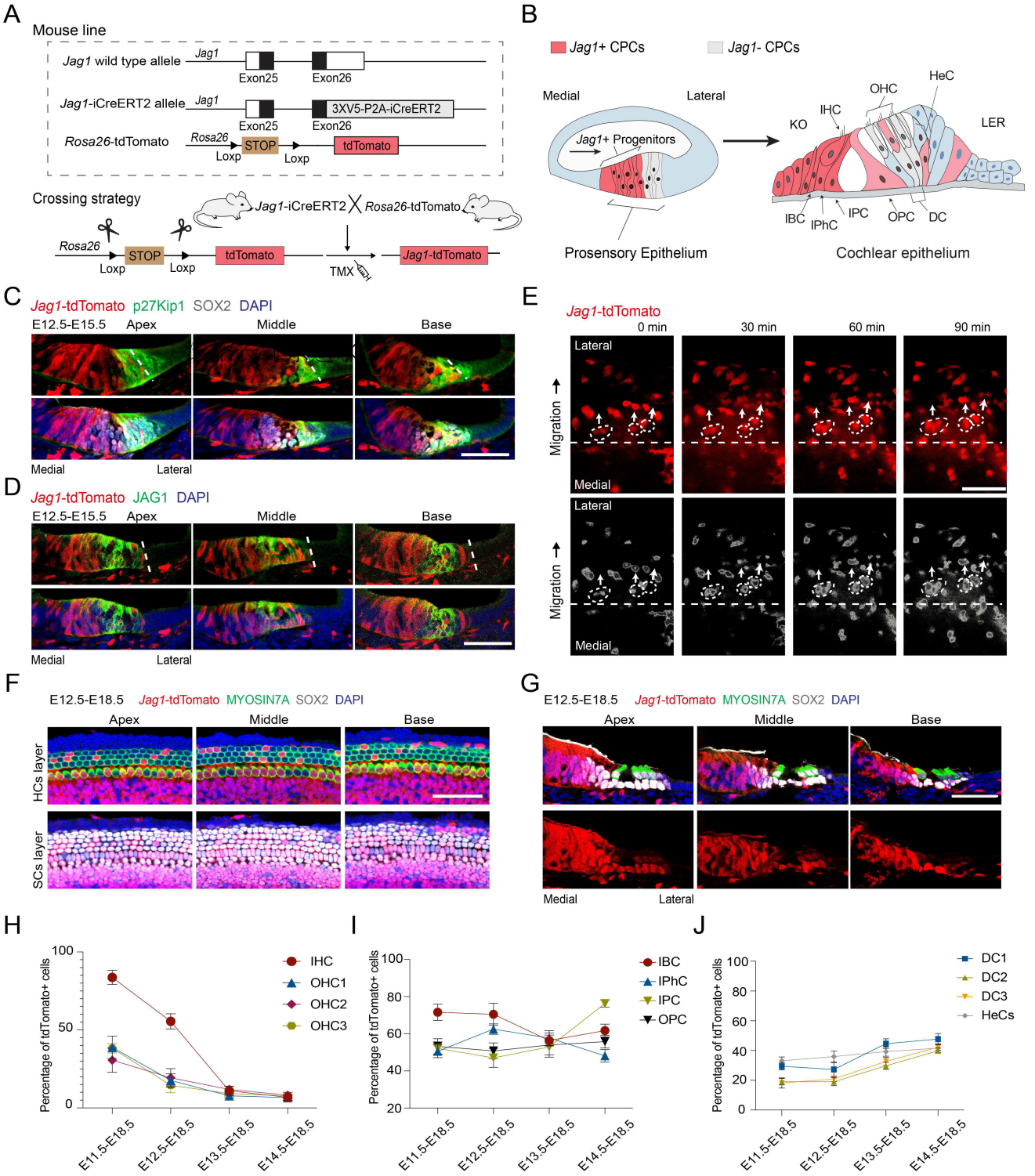


Figure 4. Lineage Tracing of *Jag1*⁺ CPCs in the Cochlear Prosensory Epithelium. (A) Strategy for *Jag*1-iCreERT2 allele targeting and genetic crossing for lineage tracing of *Jag1*⁺ CPCs. (B) Expression pattern of *Jag1* in the prosensory epithelium and lineage-traced distribution of *Jag1*⁺ CPCs within the organ of Corti. (C, D) Immunofluorescence of p27Kip1, and DAPI in *Jag1*-iCreERT2; *Rosa26*-tdTomato cochlear epithelium harvested at E15.5 following tamoxifen induction at E12.5. The white dashed line indicates the lateral boundary of Sox2⁺ sensory domain. Scale bar: 50 μm. (E) Live imaging of *Jag1*-iCreERT2; *Rosa26*-tdTomato cochlear epithelium at E14.5 after tamoxifen induction at E12.5. The horizontal dashed line marks the initial position of the tracked cells at baseline. The dashed circle highlights the representative cell being tracked. Arrows indicate the direction of cell migration. Scale bar: 50 μm. (F, G) Immunostaining for MYOSIN7A, SOX2, and DAPI in *Jag1*-iCreERT2; *Rosa26*-tdTomato cochlear epithelium at E18.5 following induction at E12.5. Scale bars: 50 μm. (H-J) Quantification of tdTomato-labeled HCs (H), medial SCs (**i**) and lateral SCs (**j**). Data are presented as means ±SEMs. (n = 6).

Cdkn1b$^+$ CPCs give rise to the lateral (abneural)cochlear epithelium and establish the medial (neural) boundary of the organ of Corti

To trace *Cdkn1b*$^+$ CPCs, we generated a *Cdkn1b*-iCreERT2 knock-in mouse model (Figure 5A, B) and crossed it with *Rosa26*-tdTomato mice. Upon tamoxifen administration at E13.5 and analysis of cochlear epithelia at E15.5, most *Cdkn1b*-tdTomato labeled cells resided in the lateral epithelium. The *Cdkn1b*-tdTomato$^+$ region exhibits partial overlap with the *Sox2*$^+$ prosensory domain, and its medial boundary resides within the *Sox2*$^+$ domain (demarcated by dashed lines; Figure 5C). This region aligned with endogenous p27Kip1 protein expression (Figure 5D), and its medial part partially overlapped with the lateral part of the JAG1$^+$ domain. Time-lapse live imaging of *Cdkn1b*-tdTomato$^+$ cells (tracing initiated at E13.5, analyzed at E15.5) demonstrated their dynamic medial migration during development (Figure 5E, Video 2).

When tamoxifen was administered at E11.5, E12.5, E13.5, or E14.5 and cochleae were analyzed at E18.5, *Cdkn1b*-tdTomato$^+$ cells were located in the lateral components of the cochlear epithelium, including the lesser epithelial ridge and the organ of Corti, with rare labeled cells in the Kölliker's organ (Figure 5F-H, Figure S4). In the organ of Corti, tracing between E12.5 and E14.5 labeled the majority of supporting cells (Figure 5F, Figure S4A). Approximately 50% of OHCs were *Cdkn1b*-tdTomato$^+$ when traced from E12.5, while over 90% of OHCs were labeled when tracing was initiated at E13.5 or E14.5 (Figure 5G, H). In contrast, IHCs were less labeled. Within the organ of Corti, the labeling efficiency of *Cdkn1b*-tdTomato decreased from lateral to medial. This gradient, combined with live imaging data of *Cdkn1b*-tdTomato$^+$ cells (Video 2), suggests medial migration of *Cdkn1b*$^+$ cells. These results demonstrate that *Cdkn1b*$^+$ prosensory cells primarily contribute to the lateral part of cochlear epithelium, including the lesser epithelial ridge and the organ of Corti, and demarcate the medial boundary of the organ of Corti during cochlear morphogenesis. This spatial and temporal lineage restriction highlights the existence of molecularly distinct prosensory subpopulations along the cochlear mediolateral axis.

Terminally differentiated cells of *Jag1*$^+$/*Cdkn1b*$^+$ CPCs populate the organ of Corti

Based on lineage tracing and single-cell RNA sequencing data, we revealed distinct spatial distribution patterns of *Jag1*$^+$ and *Cdkn1b*$^+$ CPCs, and their terminally differentiated cells, within the medial (neural) and lateral (abneural) regions of the cochlear epithelium, respectively. To label and analyze CPCs co-expressing *Jag1* and *Cdkn1b*, we developed a dual-recombinase system that simultaneously employs Cre/LoxP and Flpo/FRT technologies. We crossed *Jag1*-iCreERT2 and *Cdkn1b*-Flpo mouse lines with the *Rosa26* IS reporter line[37], which contains: 1) a STOP cassette flanked by unidirectional LoxP sites; 2) a tdTomato sequence with TGA flanked by FRT sites; and 3) a 3xGFP sequence (Figure 6A, B). In accordance with the endogenous expression patterns of *Jag1* and *Cdkn1b*, tamoxifen was administered in three consecutive doses from E12.5 to E13.5 (E12.5, E13.0 and E13.5), and cochlear epithelia were analyzed at E18.5. Upon tamoxifen induction, *Jag1*$^+$ CPCs underwent Cre-mediated excision of the STOP cassette, resulting in tdTomato expression (Figure 6C). In cells co-expressing *Jag1* and *Cdkn1b*, Flpo-mediated recombination subsequently excised the tdTomato cassette via FRT recombination, thereby activating GFP expression (Figure 6C, D). This sequential recombination strategy enabled specific fluorescent labeling of distinct CPC subpopulations. In no-tamoxifen controls, no tdTomato or GFP signal was detected in the cochlear epithelium (Figure S5A, B), confirming tight control of the *Rosa26*-IS reporter and tamoxifen-dependent recombinase activation.

At E18.5, GFP$^+$ cells were distributed throughout the organ of Corti, while tdTomato$^+$ cells were mainly localized to medial non-sensory regions (Kolliker's organ) and supporting cells (IBCs, IPhCs, and IPCs); (Figure 6E-I, Figure S5C-E). GFP labeled all major sensory cell types within the organ of Corti, including IHCs, OHCs, and their associated SCs, although the labeling efficiency varied among cell types. The selective confinement of GFP to the sensory domain (organ of Corti), with minimal non-sensory labeling (Figure S6A), demonstrates that *Jag1*$^+$/*Cdkn1b*$^+$ CPCs contribute primarily to all sensory cell types but rarely to non-sensory components. Importantly, comparative analysis of human cochlear tissues revealed conserved expression patterns, with JAG1 and p27KIP1 similarly demarcating medial and lateral prosensory domains (Figure 6J), suggesting evolutionary conservation of these fundamental mechanisms governing cochlear development. Together with live imaging data (Video 1, 2), these findings support a developmental model in which the organ of Corti is formed through coordinated contribution from distinct precursor pools, with both medial and lateral populations undergoing migration and intercalation during morphogenesis (Figure 6K).

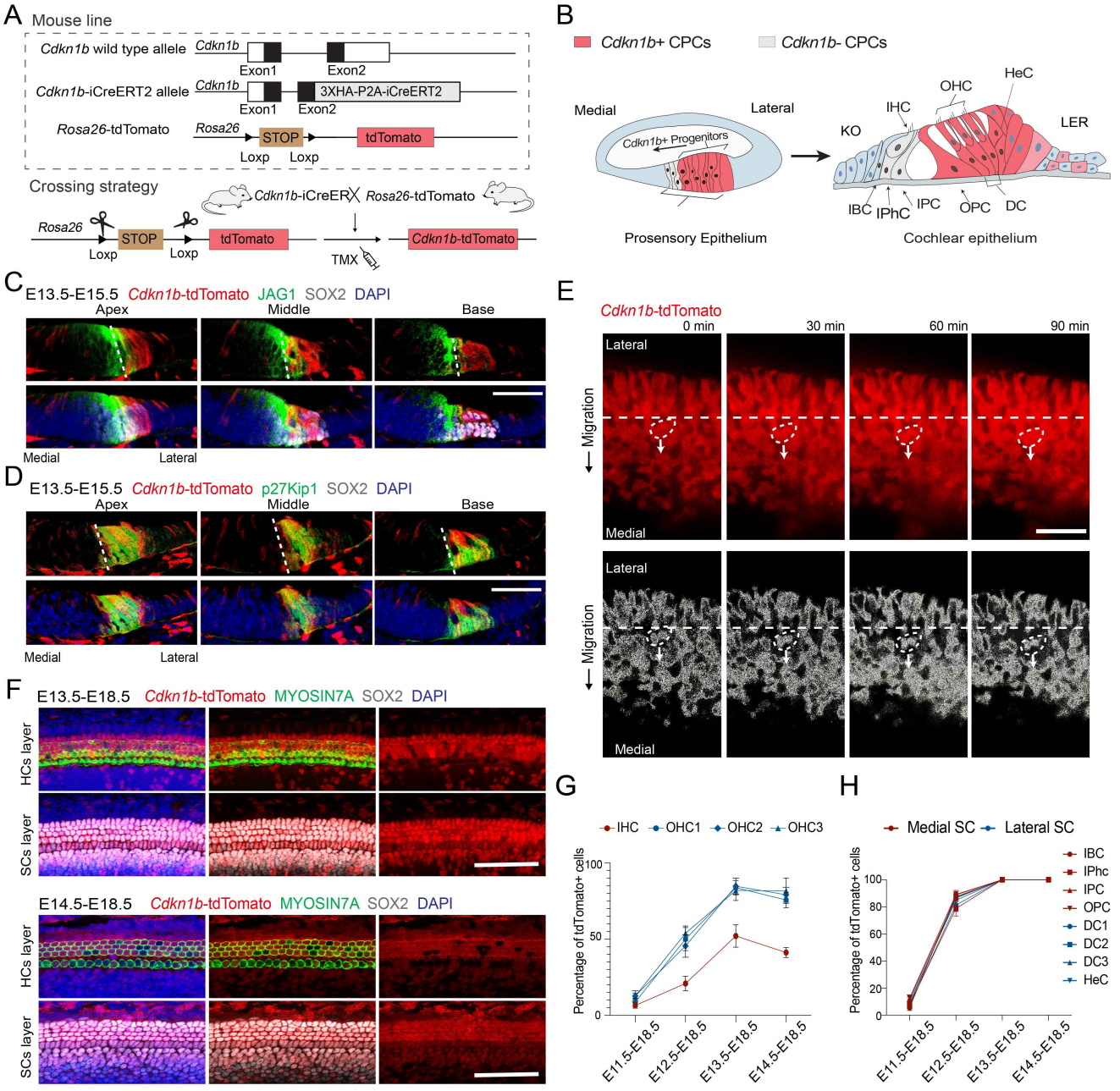


Figure 5. Lineage Tracing of *Cdkn1b*⁺ CPCs in the Cochlear Prosensory Epithelium. (A) Targeting strategy and genetic cross for lineage tracing of *Cdkn1b*⁺ CPCs using the *Cdkn1b*-iCreERT2 allele. (B) Expression pattern of *Cdkn1b* in the prosensory epithelium and lineage-traced distribution of *Cdkn1b*⁺ CPCs in the organ of Corti. (C, D) Immunostaining for JAG1 (C) and p27Kip1 (D) together with SOX2 and DAPI in the E15.5 cochlear epithelium of *Cdkn1b*-iCreERT2; *Rosa26*-tdTomato mice tamoxifen-induced at E13.5. The white dashed line indicates the medial boundary of the SOX2⁺ sensory domain in both panels (C, D). Scale bar: 50 μm. (E) Live imaging of E15.5 cochlear epithelium from *Cdkn1b*-iCreERT2; *Rosa26*-tdTomato mice after tamoxifen induction at E13.5. The horizontal dashed line marks the initial position of the tracked cells at baseline. The dashed circle highlights the representative cell being tracked. Arrows indicate the direction of cell migration. Scale bar: 50 μm. (F) Immunostaining for MYOSIN7A, SOX2, and DAPI in the middle turn of the E18.5 cochlea from *Cdkn1b*-iCreERT2; *Rosa26*-tdTomato mice after tamoxifen induction at E13.5. Scale bar: 50 μm. (G, H) Quantification of tdTomato positive HCs (G) and SCs (H). Data are presented as means ±SEMs. (n = 6).

Discussion

Our study elucidates the cellular mechanisms underlying cochlear prosensory cell specification and the formation of the Organ of Corti through the integration of single-cell transcriptomics and advanced lineage tracing approaches. We demonstrate that the seemingly uniform prosensory epithelium comprises molecularly distinct medial (*Jag1*⁺) and lateral (*Cdkn1b*⁺) CPC populations exhibiting reciprocal migratory behaviors: *Jag1*⁺ cells move laterally while *Cdkn1b*⁺ cells migrate medially through an active intercalation process that establishes the precise mediolateral organization of the mature organ of Corti (Figure 7). Furthermore, we also observed the cell delamination phenomenon where CPCs within the single-layer columnar epithelium exhibited divergent migratory patterns: some cells migrated toward the

lumen and detached from the basement membrane, while others descended toward the basement while maintaining apical protrusions that contact the luminal surface (Figure 4C, D, G, Figure 5C, D, Figure S4B).

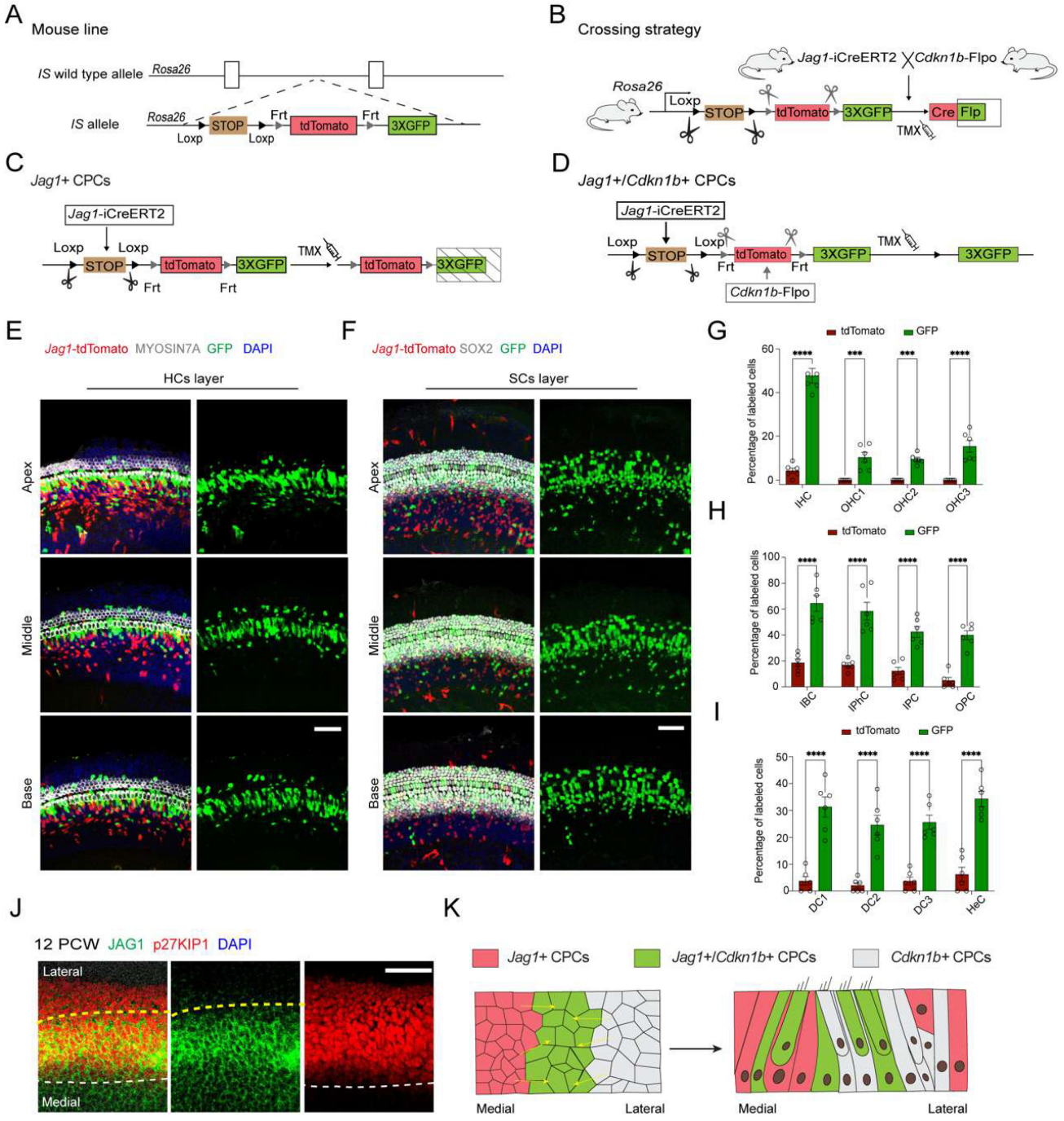


Figure 6. Dual-Recombinase Lineage Tracing of *Jag1*$^+$ and *Jag1*$^+$/*Cdkn1b*$^+$ CPCs in the developing Cochlea. (A, B) Design of the *Rosa26*-IS reporter allele and genetic strategy for tracing *Jag1*$^+$ CPCs and *Jag1*$^+$/*Cdkn1b*$^+$ CPCs. (C, D) Schematic of tdTomato labeling of *Jag1*$^+$ CPCs and GFP labeling of *Jag1*$^+$/*Cdkn1b*$^+$ CPCs in the dual-recombinase system. (E) Immunostaining for MYOSIN7A and DAPI in E18.5 cochlear epithelium from *Jag1*-iCreERT2; *Cdkn1b*-Flpo; *Rosa26*-IS mice induced with tamoxifen at E12.5, E13.0, and E13.5. Scale bar: 50 μm. (F) Immunostaining for SOX2 and DAPI in E18.5 cochlear epithelium from *Jag1*-iCreERT2; *Cdkn1b*-Flpo; *Rosa26*-IS mice induced with tamoxifen at E12.5, E13.0, and E13.5. Scale bar: 50 μm. (G–I) Quantification of *Jag1*$^+$ only and *Jag1*$^+$/*Cdkn1b*$^+$ cells across cochlear cell types: (G) HCs, (H) medial SCs, and (I) lateral SCs. Data are presented as mean ± SEM. Two-way ANOVA followed by Tukey's multiple comparisons test was used for analysis. ****$p < 0.0001$, *** $p < 0.001$ ** $p < 0.01$. (J) Expression of JAG1 and p27KIP1 in fetal human cochlear epithelium. The yellow dashed line indicates the lateral boundary, and the white dashed line indicates the medial boundary of the cochlear prosensory epithelium. Scale bar: 50 μm. (K) Proposed model of cochlear epithelial remodeling via convergent extension and radial intercalation during development.

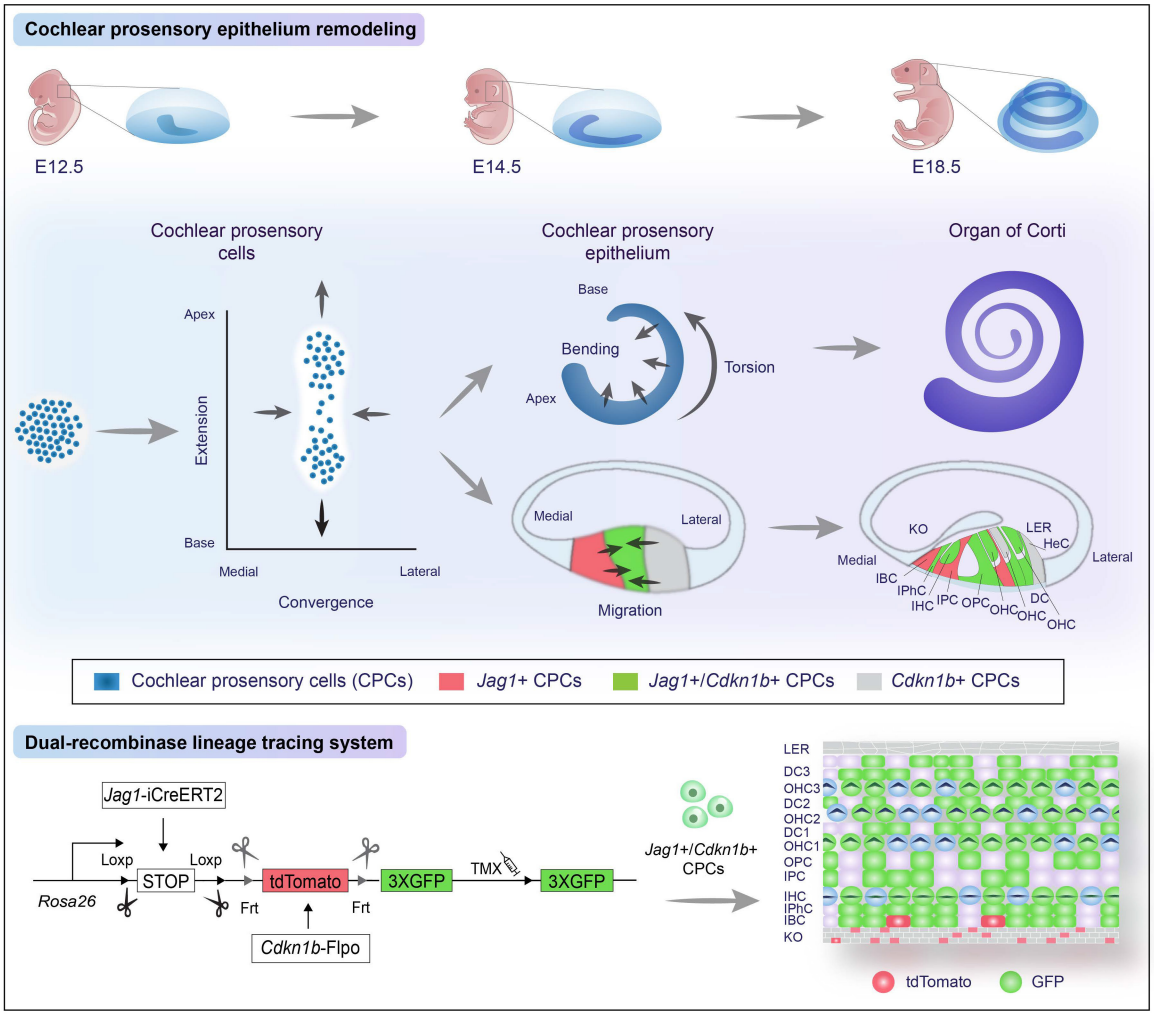


Figure 7. Schematic overview of cochlear prosensory cell patterning and organ of Corti formation. During mouse cochlear development, the seemingly uniform prosensory epithelium contains two molecularly distinct CPC subpopulations: medial (neural) *Jag1*$^+$ CPCs and lateral (abneural) *Cdkn1b*$^+$ CPCs. *Jag1*$^+$ CPCs migrate laterally, while *Cdkn1b*$^+$ CPCs migrate medially, undergoing active intercalation to establish the precise mediolateral organization of the mature Organ of Corti. *Jag1*$^+$/*Cdkn1b*$^+$ double-positive CPCs (demonstrated via dual-recombinase lineage tracing) predominantly differentiate into all sensory cell types within the Organ of Corti. Molecular signals and mechanical forces coordinate CPC migration, intercalation, and delamination.

The dual-recombinase lineage tracing system provides unprecedented resolution in mapping CPC migration dynamics. Spatial and temporal analysis reveals important developmental windows for regional specification, with *Jag1*$^+$ precursors active earlier (E11.5-E12.5) and *Cdkn1b*$^+$ populations peaking slightly later (E13.5-E14.5), mirroring the sequential differentiation of inner hair cells preceding outer hair cells (Figure S6B-C). While previous studies have identified key transcriptional regulators of hair cell fate (*Tbx2* and *Casz1* for IHCs [22,23]; *Insm1* and *Ikzf2* for OHCs [19,20,38]), the molecular mechanisms establishing initial medial (neural) -lateral (abneural) patterning of CPCs require further elucidation, as do the signals regulating their migratory behaviors. Besides, cells co-expressing *Jag1* and *Cdkn1b* predominantly contribute to all sensory cell types within the organ of Corti, representing a precisely defined and functionally committed prosensory population. The conservation of this spatial organization in human cochlear development underscores the evolutionary significance of early lineage restriction and patterning mechanisms. However, our analysis of JAG1 and p27KIP1 expression is currently limited to human cochlear specimens at 12 PCW. While these data offer valuable initial evidence for conserved molecular components, a more definitive assessment of evolutionary conservation would require dynamic expression profiling across multiple gestational stages and quantitative spatial comparisons of JAG1/p27Kip1 expression domains between mouse and human cochlear epithelia.

The processes of cochlear elongation and cellular differentiation are accompanied by region-specific patterning along both the apex-base and medial (neural) -lateral (abneural) axes. Recent studies have highlighted the pivotal roles of signaling pathways and molecular regulators, including SHH [5,39], let-

7/Lin28b [40], and Activin A (Inhba)/Follistatin (Fst) [41,42], in orchestrating the timing and spatial organization of epithelial differentiation. Strikingly, mechanical forces generated by extracellular matrix (ECM) or local cellular compression are increasingly recognized as key drivers of cochlear morphogenesis. Shear forces generated by HeCs and OHC local repulsion, mediated by MYOSIN II-dependent contractility, coordinate the intercalation and delamination of OHCs and neighboring SCs [43]. IHC positioning may result from compression by proliferating Kolliker's organ cells, which is further refined by differential cell adhesion [44]. Additionally, bending of the epithelium is driven by mechanically activated helical ERK waves triggered by cell extension [26]. Our previous work demonstrated that ECM stiffness plays a critical role in regulating the behavior of CPCs through integrin α3/F-actin/YAP signaling and PIEZO2-mediated calcium signaling [45]. These dynamic processes likely involve both cell-autonomous mechanisms and tissue-level interactions, mediated by cytoskeletal reorganization and changes in cell adhesion as revealed by the enriched expression of mechanotransduction components (*Yap1*, *Ctnnb1*, *Rhoa*) in CPCs (Figure S6D). Immunostaining further confirmed the expression of YAP1, MYOSIN2, and ITGA3 in both E13.5 CPCs and mechanically active HeCs (Figure S6E-G). These mechanosensitive elements are likely involved in mediating the medial (neural) -lateral (abneural) patterning of the cochlear epithelium, potentially by linking mechanical cues to region-specific cellular behaviors. Consistent with this, inhibition of ROCK with Y-27632 or of MYOSIN II with Blebbistatin in embryonic cochlear prosensory explants disrupted CPC reciprocal migration, leading to disorganized directionality and reduced intercalation relative to controls. These findings suggest that Rho/ROCK-dependent actomyosin contractility generates mechanical cues required for cochlear CPC migration and intercalation along the medial-lateral axis (Figure S7A, B).

In conclusion, our study establishes a new framework for understanding cochlear development, where coordinated contributions from molecularly distinct CPC populations generate the exquisite cellular patterning essential for hearing function. These findings not only advance fundamental knowledge of auditory system development but also highlight critical gaps in our understanding of initial patterning mechanisms and the regenerative potential of distinct CPC populations, pointing to the need for future studies integrating high-resolution live imaging, atomic force microscopy, and single-cell omics approaches to fully elucidate the dynamic interplay of molecular and mechanical cues shaping cochlear morphogenesis.

Materials and Methods

Single-cell RNA sequencing and analysis

The cochlear epithelium was dissociated, and sorting was performed via a MoFlo® SX FACS cytometer (Beckman Coulter). Single-cell transcriptomic profiling of the sorted living single cells was performed using the Single Cell 3' Reagent v3 kits (10X Genomics), which were then loaded on a 10x Genomics instrument to generate single-cell gel beads. Each gel bead carries a unique barcode to identify each single cell and a unique molecular identifier (UMI) to reduce PCR duplicates. In sequence, the mRNAs were subjected to reverse transcription, cDNA amplification, and library construction based on the Illumina HiSeq 4000 system. The raw 10x Genomics data were converted to FastQ format and then aligned to the mm10-mouse reference genome to generate count matrix files using Cell Ranger software (v.7.0.1). Single-cell RNA-seq profiles from embryonic day (E) 12.5 and E13.5 cochlear cells were processed in Seurat (v.4.3.0).

For cell-level quality control, we assessed total UMI counts, detected gene numbers, and mitochondrial transcript proportions per library. Our E12.5 and E13.5 datasets were filtered with fixed thresholds: ≥500 detected genes, ≥2,000 UMIs, and ≤5% mitochondrial transcripts. In contrast, publicly available E14 and E16 datasets used a lenient distribution-based filtering strategy to account for library-to-library variability in RNA content and transcriptional complexity across embryonic stages and cell populations. Cells within the main distribution were retained, while low-quality outliers with extreme UMI or gene counts (potential doublets) were discarded. After cell type annotation, 2,831 target lineage cells comprising 204 cells at E12.5, 1,322 at E13.5, 646 at E14, and 659 at E16, were retained for downstream developmental trajectory analysis (Table S3 and S4, Supporting Information).

Following normalization, identification of highly variable genes, scaling, and principal component analysis (PCA), a k-nearest neighbor graph was constructed for graph-based clustering, and the results were visualized using UMAP (commands: NormalizeData/FindVariableFeatures/ScaleData → RunPCA → FindNeighbors/FindClusters → RunUMAP).

The function "FindAllMarkers" was used to identify exclusively expressed markers of every cluster. Two or more known genes among these markers helped identify the cell type identity of every

cluster. The expression levels of the top genes of each cluster were visualized using heatmaps generated with Seurat::DoHeatmap and violin plots generated with Seurat::VlnPlot.

To define the pool of HC progenitors used for downstream trajectory inference, we subset the E12.5–E13.5 Seurat object to cells co-expressing *Epcam* and *Sox2*. Published embryonic E14 and E16 cochlear single-cell datasets were obtained from Kolla *et al.* [18], and reprocessed with the same Seurat pipeline for consistency (GEO GSE137299). We jointly analyzed four embryonic stages (E12.5, E13.5, E14, E16) using Seurat v4. For each stage-specific object, counts were normalized, and highly variable features were identified. We then selected integration features across datasets and computed anchor pairs with FindIntegrationAnchors using canonical correlation analysis (CCA). Anchors were used to create an integrated assay via IntegrateData, which corrects batch effects across time points within Seurat's anchor-based framework. After setting DefaultAssay(combined) <- "integrated", we performed ScaleData and RunPCA on the integrated matrix, constructed the neighborhood graph, and computed a UMAP embedding for visualization.

Pseudotime and lineage-associated gene discovery (Monocle 2)

Cells were subset by developmental annotation into three windows: E12.5- E13.5, E13.5- L.PsC and M.PsC- OHC and ordered with Monocle 2 (DDRTree) to reconstruct trajectories from HC progenitors toward IHC and OHC. To identify genes whose expression changes as a smooth function of pseudotime, we applied differentialGeneTest with a natural-spline model (fullModelFormulaStr = "~ sm.ns(Pseudotime)") and selected significant features at qval < [0.1]. Pseudotime-ordered heatmaps of these genes were generated using plot_pseudotime_heatmap (Monocle 2) after row-centering and clustering.

Data availability

Data have been deposited in the Gene Expression Omnibus database (scRNA-seq, GEO: GSE283476). All other data are included in the manuscript or supporting information.

Mouse models and lineage tracing

The *Jag1*-iCreERT2, *Cdkn1b*-iCreERT2, and *Cdkn1b*-Flpo mouse lines were generated in our lab via CRISPR/Cas9-mediated homologous recombination. *Rosa26*-tdTomato mice (strain #: 007909) were purchased from The Jackson Laboratory. The *Rosa26*-IS mice were kindly provided by Prof. Miao He of Fudan University. All animals were on a C57BL/6 background and housed in the Department of Laboratory Animal Science at Fudan University. All experimental procedures were approved by the Institutional Animal Care and Use Committee of Fudan University. Genotyping was performed by PCR using tail DNA to confirm the presence of the transgenes; primer sequences are provided in Table S1 (Supporting Information).

For lineage tracing of *Jag1*$^+$ or *Cdkn1b*$^+$ CPCs, adult male *Jag1*-iCreERT2 or *Cdkn1b*-iCreERT2 mice (2–4 months old) were crossed with adult female *Rosa26*-tdTomato reporter mice. Tamoxifen diluted in corn oil was injected intraperitoneally at a dosage of 4mg per 25g body weight at E11.5, E12.5, E13.5, or E14.5 to induce recombination. To trace *Jag1*$^+$/*Cdkn1b*$^+$ CPCs, adult female *Jag1*-iCreERT2; *Cdkn1b*-Flpo double-transgenic mice (2–4 months old) were mated with adult male *Rosa26*-IS reporter mice. Tamoxifen diluted in corn oil was injected intraperitoneally at E12.5, E13.0 and E13.5 to induce recombination. Vaginal plugs were checked every morning to confirm mating.

Cochlear epithelium harvesting and cryosectioning

Harvested mouse and human cochlear tissues were fixed in 4% paraformaldehyde for 6 hours at room temperature. For whole-mount staining, the basilar membrane was carefully isolated by forceps, and the stria vascularis was removed before immunohistochemistry. For cryosections, the inner ears were dissected, and serially dehydrated in 15%, 20%, and 30% sucrose before being immersed in optimal cutting temperature compound. After infiltration, the cochleae were flash-frozen with liquid nitrogen and sectioned using a Leica cryostat with sections cut at a thickness of 15 μm for subsequent immunofluorescence staining.

Immunofluorescence staining and confocal microscopy imaging

The slides or basilar membrane were permeabilized and blocked for 1 hour at room temperature in PBS with 1% Triton X-100 and 10% fetal bovine serum, followed by primary antibody incubation overnight at 4°C (antibody details are provided in Table S2, Supporting Information). PBS was then washed from the samples three times before secondary antibody incubation at room temperature for 2 hours. DAPI (1:800, 62248; Thermo Scientific™) was used to stain the nucleus. The samples were mounted using anti-fade glycerol, and confocal imaging was performed using a Leica Sp8 confocal microscope and analyzed in ImageJ and Adobe

Illustrator software.

Live imaging

The cochlear basilar membrane was cultured in a 10 mm glass-bottom dish pre-coated with Cell-Tak for 6 hours. Before imaging, the medium was replaced with pre-warmed (37 °C) DMEM/F12 phenol red-free imaging medium supplemented with 1% N2, 2% B27, and 2% ampicillin. No serum or exogenous growth factors were added during the imaging period.

For *Jag1*$^+$ CPC tracing, tamoxifen was administered at E12.5 and samples were harvested at E14.5; for *Cdkn1b*$^+$ CPC tracing, tamoxifen was administered at E13.5 and samples were harvested at E15.5. Cochlear prosensory explants were treated with the ROCK inhibitor Y-27632 (10 μM) and Blebbistatin (10 μM), a MYOSIN II inhibitor, 6 hours before imaging. The dish was then placed on a preheated microscope stage, and the environment was maintained at 37°C, 5% CO_2, and appropriate humidity using the live-cell incubation system. Image acquisition was performed using a Leica SP8 confocal microscope. Initial localization of red fluorescent proteins was conducted with low-power 561 nm laser illumination. The objective was then switched to a 40× oil-immersion lens (NA=1.3), and a highly sensitive HyD detector was employed for imaging. Laser power was kept at the minimum effective intensity (typically below 10%), and exposure time was set to less than 500 ms. Time-lapse imaging was performed at 15-minute intervals for a total duration of 1.5 hours.

Cell counts and statistical analysis

For counts of traced prosensory cells in the *Jag1*-iCreERT2; *Rosa26*-tdTomato mice, *Cdkn1b*-iCreERT2; *Rosa26*-tdTomato mice or *Rosa26*-IS; *Jag1*-iCreERT2; *Cdkn1b*-Flpo mice, tdTomato- or GFP-labeled cells were counted per 240 μm along the basilar membrane. For quantification of labeled cells along the cochlear duct, cochleae were dissected, fixed, and immunostained as described above. The cochlear duct was divided into apical, middle, and basal turns. In each turn, a 240 μm segment was selected, and the number of labeled cells and total cells of the corresponding cell type were counted within that segment. Each quantification was based on 6 embryos derived from 3 independent dams (n= 6 embryos from 3 dams per group). For each embryo, one cochlea was used for hair cell quantification and the contralateral cochlea for supporting cell quantification. Data were presented as means ± SEM. Significance of differences among cell types was calculated using an unpaired two-tailed Student's *t*-test (two groups) and one/two-way analysis of variance (ANOVA) test with multiple comparisons in GraphPad Prism software (version 10.0). P values are indicated as follows: ns, not significant, *p < 0.05, **p < 0.01, ***p < 0.001, ****p < 0.0001.

Abbreviations

CPCs: cochlear prosensory cells
HCs: hair cells
SCs: supporting cells
SHH: sonic hedgehog
RA: retinoic acid
FGF: fibroblast growth factor
IBCs: inner border cells (IBCs)
IPhCs: inner phalangeal cells
IPCs: Inner pillar cells
OHCs: outer hair cells
OPCs: outer pillar cells
DCs: Deiters cells
HeCs: Hensen cells
TC: the tunnel of Corti
PCP: planar cell polarity
GO: gene ontology
UMI: unique molecular identifier
PCA: principal component analysis
SEM: standard error of mean
ANOVA: analysis of variance

Supplementary Material

Supplementary figures, tables, video legends.
https://www.ijbs.com/v23p0705s1.pdf
Supplementary videos.
https://www.ijbs.com/v23p0705s2.zip

Acknowledgements

We thank Professor Zhiyong Liu and Professor Miao He for their assistance with the transgenic mice, as well as our team members for inspiring discussions. This work was funded by grants from the National Natural Science Foundation of China (No. 82192865, 82425018, 82192861, 82271159, 82271170, 81922018, 82192860, 82501407), the STI2030-Major Projects (No. 2022ZD0205400, 2021ZD0200100), National Key R&D Program of China (No. 2025YFC3508205, 2023YFF1204802), and the China Postdoctoral Science Foundation (No. 2025M781916).

Data availability

Data have been deposited in the Gene Expression Omnibus database (scRNA-seq, GEO: GSE283476). All other data are included in the manuscript or supporting information.

Competing Interests

The authors have declared that no competing interest exists.

References

1. Durruthy-Durruthy R, Gottlieb A, Hartman BH, Waldhaus J, Laske RD, Altman R, et al. Reconstruction of the mouse otocyst and early neuroblast lineage at single-cell resolution. Cell. 2014;157(4):964-78.
2. de Haan S, He J, Corbat AA, Belicova L, Ratz M, Vinsland E, et al. Ectoderm barcoding reveals neural and cochlear compartmentalization. Science. 2025;388(6742):60-8.
3. Xu J, Ueno H, Xu CY, Chen B, Weissman IL, Xu PX. Identification of mouse cochlear progenitors that develop hair and supporting cells in the organ of Corti. Nat Commun. 2017;8:15046.
4. Xie N, Landin Malt A, Adylkhan A, Rodeman N, Moraes Borges R, Hwang D, et al. Wnt7b acts in concert with Wnt5a to regulate tissue elongation and planar cell polarity via noncanonical Wnt signaling. Proc Natl Acad Sci U S A. 2024;121(35):e2405217121.
5. Son EJ, Ma JH, Ankamreddy H, Shin JO, Choi JY, Wu DK, et al. Conserved role of Sonic Hedgehog in tonotopic organization of the avian basilar papilla and mammalian cochlea. Proc Natl Acad Sci U S A. 2015;112(12):3746-51.
6. Duncan RK, Liu L, Moyer M, Wylie A, Dano R, Cassinotti L. Retinoic acid signaling guides the efficiency of inner ear organoid-genesis and governs sensory-nonsensory fate specification. Stem Cell Reports. 2025;20(10):102671.
7. Pirvola U, Spencer-Dene B, Xing-Qun L, Kettunen P, Thesleff I, Fritzsch B, et al. FGF/FGFR-2(IIIb) signaling is essential for inner ear morphogenesis. J Neurosci. 2000;20(16):6125-34.
8. Driver EC, Kelley MW. Development of the cochlea. Development. 2020;147(12):dev162263.
9. Montcouquiol M, Kelley MW. Development and Patterning of the Cochlea: From Convergent Extension to Planar Polarity. Cold Spring Harb Perspect Med. 2020;10(1):a033266.
10. Driver EC, Northrop A, Kelley MW. Cell migration, intercalation and growth regulate mammalian cochlear extension. Development. 2017;144(20):3766-76.
11. Qin T, So KKH, Hui CC, Sham MH. Ptch1 is essential for cochlear marginal cell differentiation and stria vascularis formation. Cell Rep. 2024;43(4):114083.
12. Sun Y, Wang L, Zhu T, Wu B, Wang G, Luo Z, et al. Single-cell transcriptomic landscapes of the otic neuronal lineage at multiple early embryonic ages. Cell Rep. 2022;38(12):110542.
13. Nikolic P, Järlebark LE, Billett TE, Thorne PR. Apoptosis in the developing rat cochlea and its related structures. Brain Res Dev Brain Res. 2000;119(1):75-83.
14. Hou S, Chen J, Yang J. Autophagy precedes apoptosis during degeneration of the Kölliker's organ in the development of rat cochlea. Eur J Histochem. 2019;63(2):3025.
15. Chen J, Gao D, Chen J, Hou S, He B, Li Y, et al. Single-Cell RNA Sequencing Analysis Reveals Greater Epithelial Ridge Cells Degeneration During Postnatal Development of Cochlea in Rats. Front Cell Dev Biol. 2021;9:719491.
16. Liu X, Xie L, Jin Y, Chen S, Shi X, Zong Y, et al. Connexin 26 Functions as a Direct Transcriptional Regulator During the Cochlea Development. Adv Sci (Weinh). 2026;13(14):e14136.
17. Wang X, Zhang L, Chen S, Xie L, Qiu Y, Kong C, et al. Viral-Mediated Connexin 26 Expression Combined with Dexamethasone Rescues Hearing in a Conditional Gjb2 Null Mice Model. Adv Sci (Weinh). 2025;12(29):e2406510.
18. Kolla L, Kelly MC, Mann ZF, Anaya-Rocha A, Ellis K, Lemons A, et al. Characterization of the development of the mouse cochlear epithelium at the single cell level. Nat Commun. 2020;11(1):2389.
19. Wiwatpanit T, Lorenzen SM, Cantú JA, Foo CZ, Hogan AK, Márquez F, et al. Trans-differentiation of outer hair cells into inner hair cells in the absence of INSM1. Nature. 2018;563(7733):691-5.
20. Chessum L, Matern MS, Kelly MC, Johnson SL, Ogawa Y, Milon B, et al. Helios is a key transcriptional regulator of outer hair cell maturation. Nature. 2018;563(7733):696-700.
21. Bi Z, Ren M, Zhang Y, He S, Song L, Li X, et al. Revisiting the Potency of Tbx2 Expression in Transforming Outer Hair Cells into Inner Hair Cells at Multiple Ages In Vivo. J Neurosci. 2024;44(23):e1751232024.
22. García-Añoveros J, Clancy JC, Foo CZ, García-Gómez I, Zhou Y, Homma K, et al. Tbx2 is a master regulator of inner versus outer hair cell differentiation. Nature. 2022;605(7909):298-303.
23. Sun Y, Ren M, Zhang Y, Li S, Luo Z, Sun S, et al. Casz1 is required for both inner hair cell fate stabilization and outer hair cell survival. Science. 2025;388(6744):eado4930.
24. Chen Y, Gu Y, Li Y, Li GL, Chai R, Li W, et al. Generation of mature and functional hair cells by co-expression of Gfi1, Pou4f3, and Atoh1 in the postnatal mouse cochlea. Cell Rep. 2021;35(3):109016.
25. Chai R, Kuo B, Wang T, Liaw EJ, Xia A, Jan TA, et al. Wnt signaling induces proliferation of sensory precursors in the postnatal mouse cochlea. Proc Natl Acad Sci U S A. 2012;109(21):8167-72.
26. Ishii M, Tateya T, Matsuda M, Hirashima T. Retrograde ERK activation waves drive base-to-apex multicellular flow in murine cochlear duct morphogenesis. Elife. 2021;10:e61092.
27. Yamamoto N, Okano T, Ma X, Adelstein RS, Kelley MW. Myosin II regulates extension, growth and patterning in the mammalian cochlear duct. Development. 2009;136(12):1977-86.
28. Koo HY, Oh JH, Durán Alonso MB, Hernández IL, González-Vallinas M, Alonso MT, et al. Analysis of Meis2 knockout mice reveals Sonic hedgehog-mediated patterning of the cochlear duct. Dev Dyn. 2025;254(4):365-72.
29. Pirvola U, Cao Y, Oellig C, Suoqiang Z, Pettersson RF, Ylikoski J. The site of action of neuronal acidic fibroblast growth factor is the organ of Corti of the rat cochlea. Proc Natl Acad Sci U S A. 1995;92(20):9269-73.
30. Najarro EH, Huang J, Jacobo A, Quiruz LA, Grillet N, Cheng AG. Dual regulation of planar polarization by secreted Wnts and Vangl2 in the developing mouse cochlea. Development. 2020;147(19):dev191981.
31. Tateya T, Sakamoto S, Ishidate F, Hirashima T, Imayoshi I, Kageyama R. Three-dimensional live imaging of Atoh1 reveals the dynamics of hair cell induction and organization in the developing cochlea. Development. 2019;146(21):dev177881.
32. Lee YS, Liu F, Segil N. A morphogenetic wave of p27Kip1 transcription directs cell cycle exit during organ of Corti development. Development. 2006;133(15):2817-26.
33. Steevens AR, Glatzer JC, Kellogg CC, Low WC, Santi PA, Kiernan AE. SOX2 is required for inner ear growth and cochlear nonsensory formation before sensory development. Development. 2019;146(13):dev170522.
34. Hao J, Koesters R, Bouchard M, Gridley T, Pfannenstiel S, Plinkert PK, et al. Jagged1-mediated Notch signaling regulates mammalian inner ear development independent of lateral inhibition. Acta Otolaryngol. 2012;132(10):1028-35.
35. Brooker R, Hozumi K, Lewis J. Notch ligands with contrasting functions: Jagged1 and Delta1 in the mouse inner ear. Development. 2006;133(7):1277-86.
36. Jiang H, Zeng S, Ni W, Chen Y, Li W. Unidirectional and stage-dependent roles of Notch1 in Wnt-responsive Lgr5+ cells during mouse inner ear development. Front Med. 2019;13(6):705-12.
37. He M, Tucciarone J, Lee S, Nigro MJ, Kim Y, Levine JM, et al. Strategies and Tools for Combinatorial Targeting of GABAergic Neurons in Mouse Cerebral Cortex. Neuron. 2016;91(6):1228-43.
38. Li S, He S, Lu Y, Jia S, Liu Z. Epistatic genetic interactions between Insm1 and Ikzf2 during cochlear outer hair cell development. Cell Rep. 2023;42(5):112504.
39. Bok J, Zenczak C, Hwang CH, Wu DK. Auditory ganglion source of Sonic hedgehog regulates timing of cell cycle exit and differentiation of mammalian cochlear hair cells. Proc Natl Acad Sci U S A. 2013;110(34):13869-74.
40. Li XJ, Doetzlhofer A. LIN28B/let-7 control the ability of neonatal murine auditory supporting cells to generate hair cells through mTOR signaling. Proc Natl Acad Sci U S A. 2020;117(36):22225-36.
41. Koo HY, Kim MA, Min H, Hwang JY, Prajapati-DiNubila M, Kim KS, et al. Follistatin regulates the specification of the apical cochlea responsible for low-frequency hearing in mammals. Proc Natl Acad Sci U S A. 2023;120(1):e2213099120.
42. Prajapati-DiNubila M, Benito-Gonzalez A, Golden EJ, Zhang S, Doetzlhofer A. A counter gradient of Activin A and follistatin instructs the timing of hair cell differentiation in the murine cochlea. Elife. 2019;8:e47613.
43. Cohen R, Amir-Zilberstein L, Hersch M, Woland S, Loza O, Taiber S, et al. Mechanical forces drive ordered patterning of hair cells in the mammalian inner ear. Nat Commun. 2020;11(1):5137.
44. Cohen R, Taiber S, Loza O, Kasirer S, Woland S, Sprinzak D. Precise alternating cellular pattern in the inner ear by coordinated hopping intercalations and delaminations. Sci Adv. 2023;9(8):eadd2157.
45. Xia M, Wu M, Li Y, Liu Y, Jia G, Lou Y, et al. Varying mechanical forces drive sensory epithelium formation. Sci Adv. 2023;9(44):eadf2664.